# Calibration of a UWB Sub-Band Channel Model Using Simulated Annealing

Jaouhar Jemai, Patrick C. F. Eggers, Gert Frølund Pedersen, and Thomas Kürner

*Abstract*—This communication presents a calibration method of an indoor UWB sub-band deterministic channel model by means of simulated annealing. Based on the characterization of the channel at sub-bands with a subset of measurement locations, the calibration optimizes the dielectric material parameters of the environment, which improves the accuracy of the model in terms of path loss ($L$) and time dispersion parameters (root mean square delay spread $\sigma_\tau$ and maximum excess delay $\tau_{\max}$) at all test locations within the test area. The performance of the calibration has been assessed by two indoor measurement campaigns, including line of sight (LOS) office and corridor and non line of sight (NLOS) corridor-office at the Antenna, Propagation and Networking Section building at Aalborg University and at the building of the Institut für Nachrichtentechnik at Braunschweig Technical University. A reasonable performance of the calibration is noticed in improving the model accuracy within the building, requiring a few pilot measurements.

*Index Terms*—Channel impulse response (CIR), material parameters, simulated annealing, sub-band divided ray tracing, UWB.

## I. OBJECTIVE AND INTRODUCTION

During the last decade, UWB communication has been gaining more interest and attracting researchers to investigate its characteristics and to develop a deep understanding of this future communication technology [1], [2]. Apart from its fine time resolution, the UWB channel is characterized by the frequency dependency of the antenna radiation patterns and of the electromagnetic material parameters. Conventional deterministic modeling methods widely used rely on tabulated values for very general elements [3]. The authors in [4] measured the reflection and transmission properties of building material slabs at UWB frequencies. However, the material parameters remain of approximate values and are difficult to define accurately for each building, especially when the materials are a heterogeneous mixture of unknown components, for which no electromagnetic measurement values are available. Consequently, blind prediction, based on *a priori* approximate knowledge of material parameters, often shows an obvious mismatch with the measurements. Therefore, an optimization method for these material parameters is required.

The main objective of this communication is to present the calibration of a sub-band deterministic UWB channel model, using a subset of a few measurements to derive more accurate channel predictions within the application area. There are some possible techniques for calibrating the model. Due to the limited measurement bandwidth, several propagation paths could arrive at the same time bin and overlap to form one path. Therefore, there is a combinatorial relationship between the path powers and the material parameters. This makes a heuristic approach based, for instance on simulated annealing, one of the most suitable ones. Moreover, the annealing method has the advantage of

tuning all material parameters (permittivity and loss tangent) simultaneously in order to optimize the defined objective function and to find the optimum by a stepped geometric decrease of the material parameters (which is not offered by other methods such as gradient, least mean square, . . .). The calibration performance has been assessed through measurement campaigns. This communication is organized as follows. Section II presents an overview of UWB deterministic channel modeling. Section III focuses on the deterministic modeling of the indoor UWB channel through ray tracing prediction using a sub-band combining technique. Section IV addresses the calibration issues and their practical implementation. The calibration performance is investigated in Section V by means of measurement campaigns.

## II. TOWARDS IMPROVING THE MODELING ACCURACY VIA CALIBRATION

The UWB channel modeling has been investigated by many authors [5]–[8]. These authors focused on the reconstruction of the channel characteristics with the existing *a priori* frequency dependency of the measured material parameters. It is noteworthy that the modeling accuracy depends on the details included in the database. However, the consideration of extensive details [9] needs more computational resources which might not even improve the accuracy of the model. There are very few publications addressing the deterministic modeling calibration issue. In [10], measurements with 200 MHz bandwidth centered at 1 GHz have been conducted and a separate tuning of the dielectric permittivity of each building wall has been performed, without considering the loss tangent. The authors presented a comparison between their model and the measurements for path loss parameters. Apart from the high computation time, the disadvantage of this method is that it provides a local minimum and not necessarily the best area solution, as it looks for the optimal values of each wall permittivity separately. In this communication, the different building structures (walls, doors, windows, . . .) are grouped into a reduced number of classes with similar physical properties (construction materials). The performance of the calibration has been assessed in conjunction with the sub-band technique. The sub-band technique is an improved approach of the one in [5]. In this communication, the model includes the frequency dependency of the antenna radiation patterns and of material parameters, which have been calibrated at each sub-band.

## III. ULTRAWIDEBAND SEMI-DETERMINISTIC SUB-BAND PREDICTION MODEL

This section describes the building database, the antenna model, the ray tracing, and the sub-band deterministic modeling technique.

### A. Building Database

The model requires an accurate 3-D indoor database with detailed information describing the scattering objects (walls, doors and windows), their thickness and their dielectric properties: The relative dielectric constant $\varepsilon_r$ and the loss tangent $\tan \delta$. According to their electromagnetic material properties, the structures of the building are classified into N different classes with common dielectric material parameters. The number of classes to use is defined depending on the variety and types of structures present in the building.

### B. Ray Tracing

The ray tracer performs a geometric and an electromagnetic computation to derive the geometrical paths and the corresponding power delay profiles (PDPs) for any transmitter and receiver position. Besides free space propagation, the propagation tool computes the Fresnel equations, considering multiple reflections and transmission

through walls. Interactions up to the 3rd order reflection have been considered. Many simulations have confirmed that this order provides a compromise between the accuracy of channel parameter (path loss and delay dispersion) and the reasonable computation time, which is also in accordance with [11]. Moreover, the model accounts for the single diffraction using the uniform theory of diffraction (UTD) [12]. For both horizontal and vertical antenna polarizations, the system considers the angle of departure (AoD) and angle of arrival (AoA) corresponding to each path, when computing the power of multipath components (MPCs). Only interactions with objects, the size of which is much greater compared to the largest wavelength within the signal, have been considered. The channel could be represented as a tapped delay line expressed by

$$h(t, \tau) = \sum_{i=1}^{P} a_i(t)\delta(\tau - \tau_i) \qquad (1)$$

where $P$ is the number of taps, $a_i(t)$ and $\tau_i$ are the complex amplitude coefficient and time of arrival (ToA) of the $i$th tap. Each of the $P$ taps corresponds to a set of MPCs which are coming closely spaced in time. As the system bandwidth is generally limited, each group of closely spaced MPCs has been represented with a particular tap delay. The channel impulse response (CIR) could then be written as

$$h(t, \tau) = \sum_{i=1}^{P} \sum_{n=1}^{i_n} a_{i_n}(t)\delta(\tau - \tau_i) \qquad (2)$$

whereby $i_n$ is the number of MPCs clustered together to form the tap $i$. Assuming wide sense stationarity and uncorrelated scattering (WSSUS), all paths are independently fading and their average power is time and space independent. This implies averaging over a local area of a selected measurement grid as shown later in Section V.

### C. Sub-Band Divided Ray Tracing

The UWB frequency bandwidth BW is divided into $n$ equal and adjacent sub-bands with $(\mathrm{BW}/n)$ bandwidth $((\mathrm{BW}/n) \leqslant 500 \text{ MHz})$ each. The simplifying assumption that material parameters and antenna radiation patterns are invariant and nonfrequency selective over a bandwidth $(\mathrm{BW}/n)$ has been made. The bandwidth limit of 500 MHz has been chosen since it enables wideband assumption according to the Federal Communication Commission (FCC) and to the standardization specifications of IEEE 802.15.4 [1]. The channel is modeled at each frequency sub-band $(\mathrm{BW}/n)$ and the frequency channel responses are afterwards deduced from the CIRs with uniformly distributed phases for the propagation paths using the Fourier transform. Hence, the resulting frequency channel response is computed by concatenating all extracted complex frequency responses. The resulting CIR is deduced via the inverse Fourier transform (IFFT). In this communication, the UWB CIR is the combination of the antenna IR and the medium IR. The total phase component resulting from the antenna and the MPCs is assumed to be uniformly random distributed. An average PDP is derived for the combined channel transfer function.

### D. Antenna Modeling

Since typically only 2-D radiation patterns (horizontal and vertical) are available, the developed model can derive a 3-D antenna radiation pattern through a bilinear interpolation knowing the measured 2-D patterns in E- and H-planes [13]. Moreover, for a better accuracy, the system model also supports 3-D measured antenna patterns at each sub-band of $(\mathrm{BW}/n)$.

## IV. CHANNEL MODEL CALIBRATION

The calibration method presented in this section has been applied earlier by the authors to calibrate WLAN [14] and wideband channel

models with 100 MHz bandwidth around 2.45 GHz [15]. This technique is applied in this communication to the UWB channel at each sub-band.

The algorithm looks for the dominant paths (for instance the once reflected paths) above the noise threshold. It identifies the same times of arrival in the PDPs and their corresponding power. The structures contributing to theses paths have their material parameters as input to the annealing algorithm.

The simulated annealing is derived from the physical heating of a material. This material is subjected to high temperature and then gradually cooled. The gradual cooling allows the material to cool to a state in which there are few weak points [16]. It achieves a kind of global optimum wherein the entire object achieves a minimum energy structure. If the material is rapidly cooled, some parts of the object are easily broken (areas of high energy structure). With rapid cooling, the object has achieved some local areas of optimal strength, but is not strong throughout. The algorithm considers a subset of $M$ measurements with $P_i$ power taps from each measurement $i$ and $N$ classes of indoor structures. The optimized objective function, defined as the root mean square error between the measured and the predicted tap powers from all $M$ measurements, is computed at each iteration $k = i \cdot j$ as

$$E_k = \frac{1}{M} \sum_{i=1}^{M} \frac{1}{P_i} \sqrt{\sum_{j=1}^{P_i} ((a_{ij})^2_{\mathrm{mod}} - (a_{ij})^2_{\mathrm{meas}})^2_k}. \qquad (3)$$

The parameters $(a_{ij})^2_{\mathrm{mod}}$ and $(a_{ij})^2_{\mathrm{meas}}$ denote the predicted and measured power of the $j$th MPC from the $i$th measurement. The algorithm starts changing the material parameters with great steps to avoid being prematurely trapped in a local minimum. It runs for $L$ steps with unchanged temperature. Subsequently, the temperature is decreased at a stepped geometric decrease factor $A$ until it approaches to zero. The algorithm stops after a certain number of steps $ST$ if there is no significant change in the objective function. After termination, the final configuration is taken as the solution. The temperature is referred to as control factor. In the calibration algorithm, the changing step is variable. It begins, e.g., with the permittivity step of 3 and ends at $10^{-2}$. These parameters have been defined by means of Monte Carlo simulations. After termination, the final configuration is taken as the solution of the problem at hand. Fig. 1 details the implemented algorithm, where $s$ is a random array of electromagnetic parameters assigned to the different structures. By decreasing the step, it computes the best value at each iteration as depicted in Fig. 2 with $50 \times 50$ iterations. The objective function evolves from 5 dB to an optimal value of 1.3 dB for which the material parameters of the database are changed. For the sub-band model, this process starts at the central frequency. A linear variation with frequency of material parameters has been considered as additional input parameter for the calibration algorithm. By the same simulated annealing technique, material parameters at the different frequencies have been computed.

## V. MEASUREMENT CAMPAIGNS AND CALIBRATION PERFORMANCE

### A. APNet Building

*1) UWB Measurement Setup and Methodology:* The measurements have been conducted at Antennas, Propagation and Radio Networking (APNet) Section at Aalborg University (Denmark) in frequency domain using a vector network analyzer (VNA), which sweeps the radio channel in the range 2–6 GHz. The transmit power is set at 0 dBm and no amplifier was used in the system as short ranges have been considered. The CIR is derived from the inverse Fourier transform (IFFT) of the measured transfer function. The use of 801 frequency points with 5-MHz frequency steps yields a maximum ToA of 200 ns. To reduce the leakage while preserving a good resolution, a Hamming filter has been employed. By keeping both Tx and Rx stationary in a fixed environment with static scatterers, the channel can be treated as
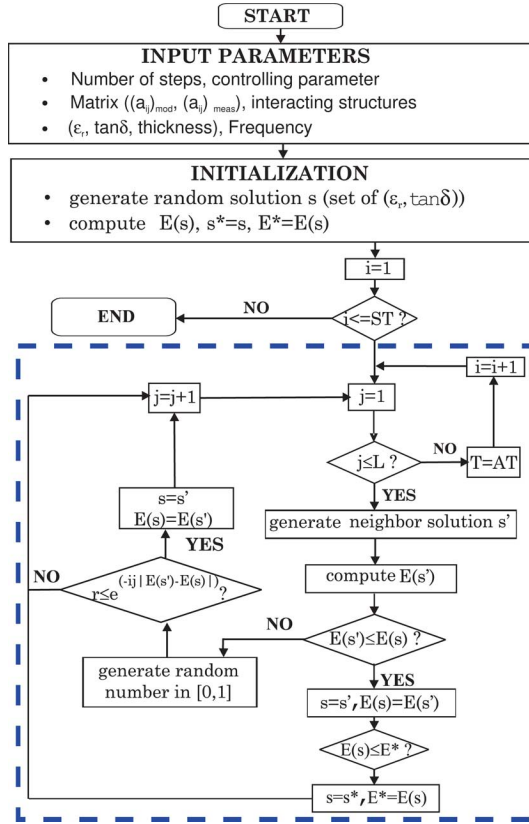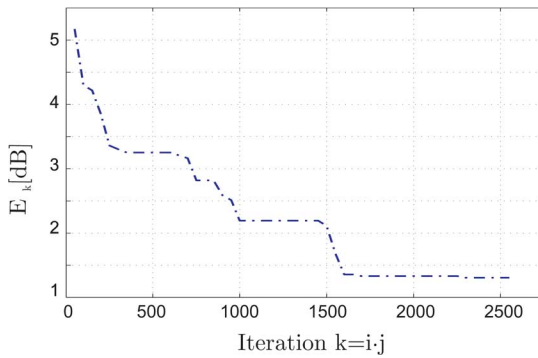
Fig. 1. Flowchart of the simulated annealing algorithm.



Fig. 2. Objective function variation with $50 \times 50$ iterations $(A = 0.97)$.



Fig. 3. Three-dimensional view of the APNet building with 1st order reflection.
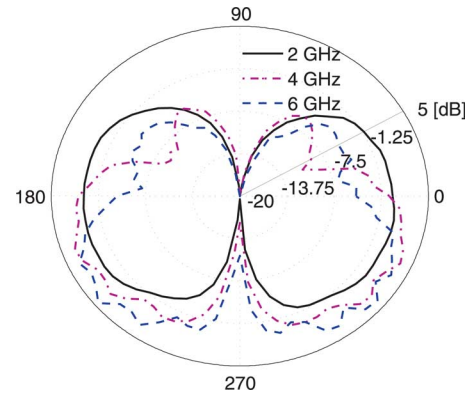


Fig. 4. Measured 2-D vertical patterns at 2, 4, and 6 GHz.

being quasi-stationary. In order to measure a locally averaged CIR, the small scale fading is suppressed via averaging over several uncorrelated CIRs, taken from a representative local area (grid). In this communication, validation measurements have been conducted with different grid sizes of $7.5 \times 7.5$ cm, $45 \times 45$ cm, and $100 \times 100$ cm, with 2.5-cm spacing between adjacent points (corresponding to the half of the smallest wavelength $\lambda$). The variation of the spatial correlation of PDPs has been analyzed with varying grid size and delay zones of the first 10 ns, 50 ns, and the entire profile at the lowest frequency. Early components, arriving within 10 ns, show a correlation amounting to 0.7. Later components exhibit much less correlation. The entire received CIR exhibits a correlation of 0.2 with the small grid. Uncorrelated delay profiles are noticed similarly for the $7.5 \times 7.5$ cm and for the $45 \times 45$ cm grids for this environment. At higher frequencies the PDPs are even lower correlated using the small grid. Hence, a compromise between ensuring uncorrelated multipath for averaging, preserving tap
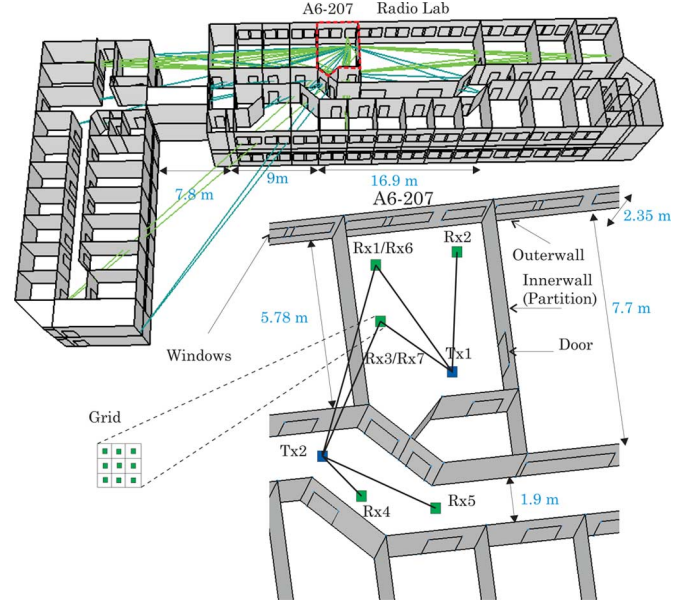
stability and stationarity has to be fulfilled. This would preserve the representativeness of the measurement location for small Tx-Rx distances (3.3–5.5 m) while keeping the measurement time reasonably low for each location. Therefore, a grid of $7.5 \times 7.5$ cm has been considered in this case. The position Tx1 (see Fig. 3) corresponds to LOS intraoffice measurements, whereas position Tx2 is for both LOS corridor and NLOS corridor-office measurements.

*2) Modeling and Calibration Performance:* Fig. 3 displays a 3-D perspective view of the building, where the measurement campaign has been conducted [17]. The dielectric parameters $(\varepsilon_r, \tan \delta)$ for blind predictions have been taken from measurement results presented in [4]. An omnidirectional UWB discone antenna with a measured pattern shown in Fig. 4 at 2, 4, and 6 GHz has been used. The ray tracing propagation model has been calibrated using a subset of three LOS intraoffice measurements within the room 207 (Tx1-Rx1, Tx1-Rx2, and Tx1-Rx3) as shown in Fig. 3. Generally, the material parameters vary slightly over a frequency range of 4 GHz. This has been confirmed in [18], [4]. Generally, the calibration results has shown low varying parameter values. Fig. 5(a) and (b) are plots of the PDP at locations Tx1-Rx1 for LOS intraoffice before and after calibration. The transmitter-receiver distance was at 3.5 m. The PDPs are plotted for a range up to 50 ns in order to better visualize the different MPCs. An improvement of channel parameter estimation is shown in Table I. The calibrated model derives
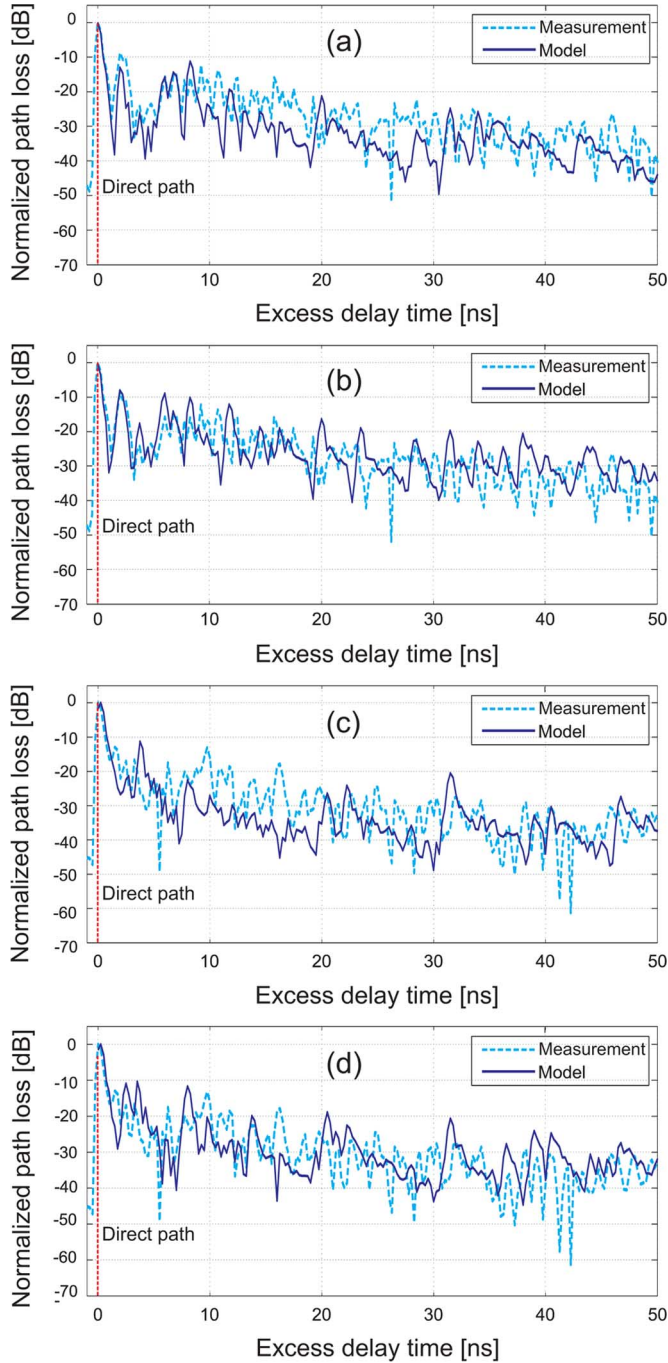
Fig. 5. Power delay profile at (a) Tx1-Rx1 prior to calibration, (b) Tx1-Rx1 after calibration, (c) Tx2-Rx4 prior to calibration, and (d) Tx2-Rx4 after calibration.

TABLE I
LOS OFFICE (USED FOR CALIBRATION)

| Position | Param. | Meas. | Uncal. | Cal. |
|----------|--------|-------|--------|------|
| Tx1-Rx1 | $\sigma_\tau$ [ns] | 6.7 | 2.6 | 7.2 |
|         | $\tau_{max}$ [ns] | 48.3 | 33.4 | 52.3 |
|         | $L$ [dB] | 53 | 55.7 | 55.4 |
| Tx1-Rx2 | $\sigma_\tau$ [ns] | 4.8 | 3 | 5 |
|         | $\tau_{max}$ [ns] | 35.5 | 20 | 29 |
|         | $L$ [dB] | 47.9 | 51 | 50.8 |
| Tx1-Rx3 | $\sigma_\tau$ [ns] | 6.2 | 3.5 | 6.5 |
|         | $\tau_{max}$ [ns] | 46 | 25.8 | 35 |
|         | $L$ [dB] | 51.3 | 55 | 54.2 |

TABLE II
LOS CORRIDOR (NOT USED FOR CALIBRATION)

| Position | Param. | Meas. | Uncal. | Cal. |
|----------|--------|-------|--------|------|
| Tx2-Rx4 | $\sigma_\tau$ [ns] | 6.7 | 3.6 | 6.4 |
|         | $\tau_{max}$ [ns] | 50.5 | 32.1 | 42 |
|         | $L$ [dB] | 55.6 | 57.3 | 57.1 |
| Tx2-Rx5 | $\sigma_\tau$ [ns] | 4.7 | 2.87 | 4.4 |
|         | $\tau_{max}$ [ns] | 38.5 | 31.75 | 40.5 |
|         | $L$ [dB] | 49.3 | 50.8 | 49.9 |

TABLE III
NLOS CORRIDOR-OFFICE (NOT USED FOR CALIBRATION)

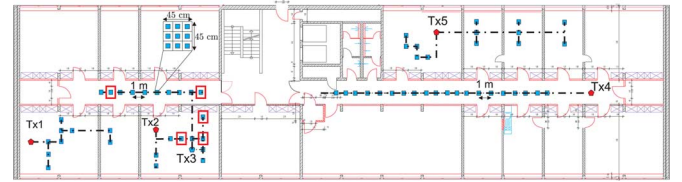| Position | Param. | Meas. | Uncal. | Cal. |
|----------|--------|-------|--------|------|
| Tx2-Rx6 | $\sigma_\tau$ [ns] | 11.7 | 15.7 | 9.9 |
|         | $\tau_{max}$ [ns] | 75.5 | 98.5 | 80.1 |
|         | $L$ [dB] | 62.6 | 59 | 60.5 |
| Tx2-Rx7 | $\sigma_\tau$ [ns] | 13.2 | 6.6 | 13.7 |
|         | $\tau_{max}$ [ns] | 91.25 | 42.25 | 105.5 |
|         | $L$ [dB] | 64.5 | 59.7 | 61.5 |



Fig. 6. Indoor office building measurement locations.

has only used the LOS intraoffice measurements presented in Table I, the calibrated model outperforms the standard model for other positions in the test area not considered in the calibration. The results given in Tables II and III show the robustness of the performed calibration. The accuracy of the channel model has been particularly improved in terms of time dispersion (by factor of 2 to 3) while path loss parameter changes are insignificant in the shown cases (rarely over 1 dB).

### B. IfN Building

In order to further investigate the calibration issue for the UWB channel, a second extensive measurement campaign has been conducted at the building of the Institut für Nachrichtentechnik (IfN) at Braunschweig Technical University (Germany) in the frequency domain using a VNA in the range of 3–8 GHz (5-GHz bandwidth) with a number of frequency points of 1601 giving a time delay of 320 ns. An intermediate frequency bandwidth of 300 Hz and a sweep time of 9.6 s are considered. An active amplifier, an HF-relay and a directional coupler have been used to sound the channel with a transmit power of 0 dBm. A number of $66 \times 9$ measurements have been conducted [19] as illustrated in Fig. 6. To derive averaged local power delay profiles, a grid of nine measurements $45 \times 45$ cm has been considered. The bandwidth of 5 GHz has been divided into ten sub-bands with 500 MHz each. As the building materials are heterogeneous, the

quite closer maximum excess delay and delay spread values. The measured path loss is 53 dB, whereas the predicted one before and after calibration amounts to 55.7 dB and 55.4 dB, respectively. In this case, the change in path loss is insignificant. As the main objective of the calibration is to get a robust model which performs well at any location (including those not used for the calibration), measurements have been conducted on the corridor where Tx2 and Rx4 have a distance of 4.4 m to each other. Fig. 5(c) and (d) shows the PDP for LOS corridor before and after calibration with a focus on the time domain up to 50 ns. The calibrated model achieves a good performance in estimating the maximum excess delay and the delay spread. Though the calibration

TABLE IV
MODEL ERROR STATISTICS PRIOR TO CALIBRATION

| Config. | 5 Measurements calibration set | | 61 Measurements test set | |
|---|---|---|---|---|
| Statistic | mean | std | mean | std |
| L [dB] | -1.6 | 4.3 | 1.9 | 5.5 |
| $\sigma_\tau$ [ns] | 4 | 3.9 | 1.6 | 7.5 |
| $\tau_{max}$ [ns] | -10.1 | 33.3 | -29.9 | 46 |

TABLE V
MODEL ERROR STATISTICS CALIBRATED WITH FIVE MEASUREMENTS

| Config. | 5 Measurements calibrating | | 61 Measurements not calibrating | |
|---|---|---|---|---|
| Statistic | mean | std | mean | std |
| L [dB] | -0.2 | 2.1 | 0.4 | 3.8 |
| $\sigma_\tau$ [ns] | -0.6 | 1.6 | -2.1 | 3.3 |
| $\tau_{max}$ [ns] | -1 | 13.7 | -24.2 | 16.6 |

parameters for the $N = 20$ structure classes are introduced according to tabulated values in [4].

The calibration has been performed using a set of five measurements relative to the transmitter Tx2 (3 LOS and 2 NLOS) marked with squares in Fig. 6. These measurements have been chosen to be representative of the entire floor plan. The performance of the calibrated model has been assessed with the complete set of 66 measurements prior to calibration and after calibration. Tables IV and V evaluate the model performance (in terms of mean and standard deviation error regarding the measurement data) for the subset of five measurements and for the remaining 61 measurements prior to and after calibration. According to Table IV, the five measurements used for the calibration are neither the best nor the worst measurements in terms of blind prediction accuracy. Though the model performs better for the five measurements considered in the calibration (as shown in Table V), it provides also very good results for the remaining 61 measurements not considered in the calibration. Generally, an overall path loss error of $-0.2$ dB and of 0.4 dB is derived for the subset of five measurements and for the rest of the measurements after calibration. This provides an error of 0.3 dB for the complete set of measurements. The standard deviations of 2.1 dB and 3.8 are noticed for the small set and for the rest of the measurements. An overall delay spread mean error of $-2$ ns with a standard deviation after calibration of 3.2 ns is computed. As the MPCs are closer to the measurements, more accurate values are also derived for the maximum excess delay shown by a mean error of $-23.1$ ns with a standard deviation of 16.4 ns. Consequently, both mean deviation and variation in time dispersion as well as power are reduced, using our calibration procedure.

Though it does consider neither the complete environment details with its small objects, nor the diffuse scattering due to rough surfaces, as investigated, e.g., in [20], the calibrated model provides a better accuracy, which is achieved by considering only approximately 10% of the measurement data for calibration.

## VI. CONCLUSION

This communication addresses a calibration procedure, based on simulated annealing, used to calibrate an UWB sub-band divided model. This method has the advantage of tuning all parameters (permittivity and loss tangent) simultaneously to reduce the mismatch between the model and the measurements. Only a few pilot measurements, which consist of a small fraction of 10% of the measurement set, are required to adjust the channel parameters, while statistical models would need more than 50% of the complete measurement set for the fitting [19]. This technique is very helpful in terms of planning and site survey aspects. While a statistical model would need extensive measurement campaigns to fit a certain variation, the calibration of the deterministic model requires a subset of measurements at repre-

sentative locations in the building and provides more accurate channel parameters at any other position. The aim of the calibration procedure presented in this communication is to calibrate the parameters of a building the structures of which are involved in the calibration set itself and not a one with totally different structures, which would be a totally blind application beyond the aim of the communication. Therefore, a new area or a structure requires a new calibration set. This is a realistic assumption for the deployment of our prediction and calibration algorithms. Further improvement of the ray tracing model is possible by considering diffuse scattering of radio waves due to small interacting objects and rough surfaces within the indoor environment.

## REFERENCES

[1] B. Allen, M. Dohler, E. Okon, W. Malik, A. Brown, and D. Edwards, *Ultra-Wideband Antennas and Propagation for Communications, Radar and Imaging*. Hoboken, NJ: Wiley, 2006.

[2] A. Molisch *et al.*, "A comprehensive standardized model for ultrawideband propagation channels," *IEEE Trans. Antennas Propag.*, vol. 54, no. 11, pp. 3151–3166, Nov. 2006.

[3] W. Malik and D. Edwards, "Spatio-temporal ultrawideband indoor propagation modelling by reduced complexity geometric optics," *IET Commun. Lett.*, vol. 1, no. 4, pp. 751–759, Jun. 2007.

[4] A. Muqaibel *et al.*, "Ultrawideband through the wall propagation," in *Proc. IEEE Micr., Antennas Propag.*, Dec. 2005, vol. 152, no. 6, pp. 581–588.

[5] H. Sughara *et al.*, "Development and experimental evaluations of RS-2000—A propagation simulator for UWB systems," in *Proc. IEEE UWBST*, 2004, pp. 76–80.

[6] W. Malik, D. Edwards, and C. Stevens, "Frequency dependence of fading statistics for ultrawideband systems," *IEEE Trans. Wireless Commun.*, vol. 6, no. 3, pp. 800–804, Mar. 2007.

[7] W. Soergel and W. Wiesbeck, "Influence of the antennas on the ultrawideband transmission," in *EURASIP J. Appl. Signal Process.*, Mar. 2005, pp. 297–305.

[8] R. Qiu, "A generalized time domain multipath channel and its application in ultra-wideband (UWB) wireless optimal receiver design—Part II: Physics-based system analysis," *IEEE Trans. Wireless Commun.*, vol. 3, no. 6, pp. 2312–2324, Nov. 2004.

[9] G. Athanasiadou and A. Nix, "A novel 3-D indoor ray-tracing propagation model: The path generator and evaluation of narrow-band and wideband predictions," *IEEE Trans. Veh. Technol.*, vol. 49, no. 4, pp. 1152–1168, Jul. 2000.

[10] J. Beneat and N. Bailey, "Optimization of building materials for accurate indoor ray tracing models," in *Proc. IEEE MILCOM Conf.*, Oct. 2004, vol. 13, no. 4, pp. 562–566.

[11] R. A. Valenzuela, S. Fortune, and J. Ling, "Indoor propagation prediction accuracy and speed versus number of reflections in image-based 3-d ray-tracing," in *Proc. 48th IEEE VTC*, May 1998, vol. 1, pp. 539–543.

[12] D. A. McNamara, C. W. I. Pistorius, and J. A. G. Malherbe, *Introduction to the Uniform Geometrical Theory of Diffraction*. Reading, MA: Artech House, 1990.

[13] F. Gil *et al.*, "A 3D interpolation method for base-station-antenna radiation patterns," *IEEE Antennas Propag. Mag.*, vol. 43, no. 2, pp. 132–137, Apr. 2001.

[14] J. Jemai and T. Kürner, "Broadband WLAN channel sounder for IEEE 802.11b," *IEEE Trans. Veh. Technol.*, vol. 57, no. 6, pp. 3381–3392, Nov. 2008.

[15] J. Jemai and T. Kürner, "Calibration of indoor channel models," in *Proc. ITG/VDE*, Osnabrück, Germany, May 2007, pp. 31–36.

[16] R. V. V. Vidal, *Applied Simulated Annealing*. New York: Springer-Verlag, 1993, Lecture Notes in Economics and Mathematical Sciences.

[17] J. Jemai, P. Eggers, G. F. Pedersen, and T. Kürner, "On the applicability of deterministic modelling to UWB channels," in *Proc. WPNC*, Hannover, Germany, Mar. 2006, pp. 139–148.

[18] R. Buehrer *et al.*, Ultra-Wideband Propagation Measurements and Modeling, Tech. Rep., Virginia Tech., Jan. 2004, DARPA NETEX Program Final Rep.

[19] J. Jemai, I. Schmidt, and T. Kürner, "UWB channel: From statistical modeling to calibration-based deterministic modeling," presented at the GeMiC, Hamburg, Germany, Mar. 10–12, 2008, extended version in *Eur. Microw. J.*

[20] Y. Lostanlen and G. Gougeon, "Introduction of diffuse scattering to enhance ray-tracing methods for the analysis of deterministic indoor UWB radio channel," in *Proc. ICEAA*, Torino, Italy, Sep. 2007, pp. 903–906.